

Article

Experimental Study on the Catalytic Ignition Characteristics of a Dual-Mode Ionic Liquid Propellant in Model Thrusters

Jie Fang ^{1,2} , Zun Wang ³, Hao Yan ^{1,2}, He Gao ^{1,2}, Zhaopu Yao ^{1,2,*} and Shuiqing Li ³¹ Beijing Institute of Control Engineering, Beijing 100190, China² Beijing Engineering Research Center of Efficient and Green Aerospace Propulsion Technology, Beijing 100190, China³ Department of Energy and Power Engineering, Tsinghua University, Beijing 100084, China

* Correspondence: yzp06@sina.com

Abstract: An experimental study was carried out on the ignition characteristics of the HAN/(Emim)(EtSO₄) (hydroxylammonium nitrate and 1-ethyl-3-methyl-imidazolium ethyl sulfate) dual-mode ionic liquid monopropellant in chemical propulsion mode in model thrusters. Firstly, a model thruster with a detachable convergent nozzle was designed and fabricated. Secondly, catalytic ignition experiments at different flow rates were carried out in atmosphere and in high chamber pressure environment, respectively, using a model thruster, with and without the convergent nozzle. During the catalytic ignition process, measurement methods such as thermocouple, pressure sensor, and flue gas analyzer were employed to obtain the temperature at different depths of the catalytic bed, the pressure of the combustion chamber, and the concentration variations of gaseous products CO, CO₂, CH₄, SO₂, NO, and NO₂. Then the three characteristic stages of water evaporation, HAN decomposition, and (Emim)(EtSO₄) combustion were analyzed at the initiation time, and the reaction characteristics in the process of the catalytic ignition were analyzed. In addition, the composition and concentration of the combustion products at equilibrium were theoretically calculated. The effects of temperature and pressure on the concentrations of five main gaseous products were studied. Finally, the exhaust gas of the three groups of catalytic ignition experiments under different pressure environments was separately collected and measured with gas chromatography (GC) when the experiments approached equilibrium, the result of which roughly agrees with the theoretical calculations. These results are of great significance for exploring the chemical propulsion of the dual-mode ionic liquid propellant and understanding its physical catalytic combustion mechanisms.

Keywords: dual-mode propulsion; ionic liquid propellant; catalytic ignition; combustion; chemical propulsion; liquid space thruster



Citation: Fang, J.; Wang, Z.; Yan, H.; Gao, H.; Yao, Z.; Li, S. Experimental Study on the Catalytic Ignition Characteristics of a Dual-Mode Ionic Liquid Propellant in Model Thrusters. *Energies* **2022**, *15*, 8730. <https://doi.org/10.3390/en15228730>

Academic Editor: Agustin Valera-Medina

Received: 26 October 2022

Accepted: 15 November 2022

Published: 20 November 2022

Publisher's Note: MDPI stays neutral with regard to jurisdictional claims in published maps and institutional affiliations.



Copyright: © 2022 by the authors. Licensee MDPI, Basel, Switzerland. This article is an open access article distributed under the terms and conditions of the Creative Commons Attribution (CC BY) license (<https://creativecommons.org/licenses/by/4.0/>).

1. Introduction

Multimode space propulsion refers to the integration of two or more propulsion modes into a single propulsion system using shared propellant [1], such as the combination of monopropellant and bipropellant chemical rocket engines [2], the combination of monopropellant and electrospray propulsion, and Hall-effect (HET) system [3] which operates at either high-thrust mode or high-specific impulse mode, etc. Among them, the dual-mode space propulsion technology based on the novel ionic liquid monopropellant has received wide attention. This technology adopts the monopropellant chemical propulsion mode to realize a large thrust and attains the high specific impulse through the electrospray propulsion mode. Thus, it will provide unprecedented flexibility and adaptability to spacecraft. Moreover, the comprehensive efficiency of the shared propellant will be significantly improved and a mass saving of the propulsion system for space missions can be acquired [4,5].

As for the novel ionic liquid monopropellant, ionic liquid (IL) is a kind of molten salt, and the cations and anions are in a dissociated state. IL has some unique properties such as

liquidity over a wide temperature range, high thermal stability, structural designability, the ability to dissolve a wide range of chemical species, low vapor pressure, and ionic conductivity, etc. [6]. In 2010, Brian R. Donius [7] from Missouri University of Science and Technology presented an analytical and numerical investigation into the performance of a dual-mode propulsion system using ionic liquids, with high-thrust chemical propulsion and high-specific impulse electric propulsion, pointing out that a similar performance to traditional storable propellant combinations was possible if ionic liquids were combined with a hydroxylammonium nitrate (HAN) oxidizer. It was also suitable as an electrospray propulsion because of its negligible vapor pressure [8].

Following that, Steven P. Berg and Joshua L. Rovey conducted a continuing study. Chemical-electrospray dual-mode propulsion technology requires a liquid propellant with physical properties of high density, low melting point, low viscosity, high surface tension, high electrical conductivity, and high molecular weight. Based on the performance requirements of the electrospray propellant, the final choice was imidazole-based ionic liquids [9]. After studying (Bmim)(dca), (Bmim)(NO₃), and 1-ethyl-3-methyl-imidazolium ethyl sulfate (Emim)(EtSO₄), it was found that their physicochemical properties are no less than that of hydrazine [10] and the currently widely used (Emim)(Im) electrospray propellant. These ionic liquids had the potential to form dual-mode ionic liquid propellants when they were mixed with oxidizing salts, such as HAN, as fuels [11]. Therefore, they synthesized monopropellants in which HAN was mixed with (Bmim)(NO₃), (Emim)(EtSO₄) respectively [12], and carried out experimental studies in both electrospray and chemical propulsion. On the one hand, electrospray experiments at different flow rates in a 100 μm capillary emitter were conducted [13], on the other hand, the catalytic decomposition characteristics of the HAN/(Emim)(EtSO₄) propellant was tested on the surface of platinum, rhenium, and titanium [14], and the linear combustion rate of propellants under different pressures was measured and evaluated in a pressurized fixed volume reactor [15]. Then, a microtubule model was established to integrate the dual-mode thruster hardware device. After that, a platinum microtubule with an inner diameter of 0.4 mm was designed, in which decomposition experiments of the HAN/(Emim)(EtSO₄) propellant were carried out [16].

In 2020, based on Berg and Rovey's research, Froberg Aerospace [17] demonstrated a Monoprop-Electrospray Propulsion System (MEPS) using the shared multimode propellant FAM-110A (59% wt. HAN, 41% wt. (Emim)(EtSO₄), <1% H₂O). MEPS microthruster consists of a stainless-steel block containing a 16 by 16 emitter array. Each emitter was lined with a catalyst layer, and each had a sharpened emitter tip at the emitter exit. It can be used as a chemical monopropellant thruster and a capillary electrospray thruster and can switch between them. Two operating modes of the MEPS were tested with stable combustion times of up to 45 s in the chemical propulsion mode [17] and more than 4 h in the electrospray mode [18]. In addition, Wang [19] also prepared a series of imidazole-based ionic liquids and mixed them with the HAN to form novel ionic liquid propellants. Their physical and chemical properties were studied, and a drop test was carried out proving that the HAN/(Emim)(EtSO₄) blend propellant had good catalytic decomposition and combustion performance. It was a new multimode ionic liquid propellant with a potential application.

Previous research has carried relatively systematic work on the screening, synthesis, and physicochemical properties of dual-mode ionic liquid propellants. The feasibility of electrospray mode and chemical propulsion mode has also been explored. A dual-mode propulsion prototype has been developed and a preliminary test has been carried out. However, the propellant's working characteristics under both modes need more study. For the chemical propulsion mode, plenty of research needs to be done to figure out the catalytic combustion characteristics of the propellant, and get an in-depth understanding of the chemical reaction process of the propellant under continuous flow in the space thruster.

Recently, Gao [20] studied the thermal and catalytic decomposition of the new ionic liquid propellant with thermogravimetric experimental analysis (TGA-DSC) and analyzed the exhaust gas using Fourier transform infrared spectroscopy measurement (FTIR). A

chemical microthruster [21] was designed by the University of Illinois Urbana-Champaign, Froberg Aerospace, and the University of Southampton and then tested using FAM-110A propellant. Li [22] built a set of catalytic ignition devices, successfully ignited a dual-mode ionic liquid propellant in the atmosphere and studied its catalytic ignition characteristics. Tang [23] designed a novel ignition actuator using the plasma-assisted microwave torch to ignite an ionic liquid monopropellant. Fang [24] conducted catalytic ignition experiments of the same propellant under a vacuum environment to explore the combustion characteristics of the propellant at a flow rate of 1 mL/min~4 mL/min.

Based on the previous work [19,22,24], this research seeks to approach closer to the actual working conditions of the space thruster under chemical propulsion mode. We designed a model thruster with a detachable convergent nozzle, built an atmospheric experimental stand, and then carried out catalytic ignition experiments of a dual-mode ionic liquid propellant at different flow rates. At the same time, variations in temperature, pressure, gaseous products, and their respective concentration in the catalytic ignition progress were measured. The theoretical calculation of the combustion products at equilibrium was performed using the NASA Chemical Equilibrium with Application (CEA) code. For comparison, gas chromatography (GC) analyzed the collected gas when the reaction approached equilibrium.

2. Methodology

2.1. Model Thruster and Experimental Setup

Figure 1a displays a model thruster and the experimental stand used in the experiment. The HAN/(Emim)(EtSO₄) dual-mode ionic liquid monopropellant (a blend of (Emim)(EtSO₄), HAN and water) flows in from the upstream inlet, and the solenoid valve controls if the propellant can flow into the model thruster. Then the propellant is injected into the catalytic bed through the injector. The catalytic bed is filled with black Ir/Al₂O₃ catalysts. Differing from hypergolic ionic liquids [25,26], the HAN/(Emim)(EtSO₄) propellant needs to be preheated, so the outside surface of the catalytic bed is wound by a heating wire. When the propellant contacts the preheated catalyst, the catalyst decomposes. Then the generated gas will be discharged through the downstream outlet.

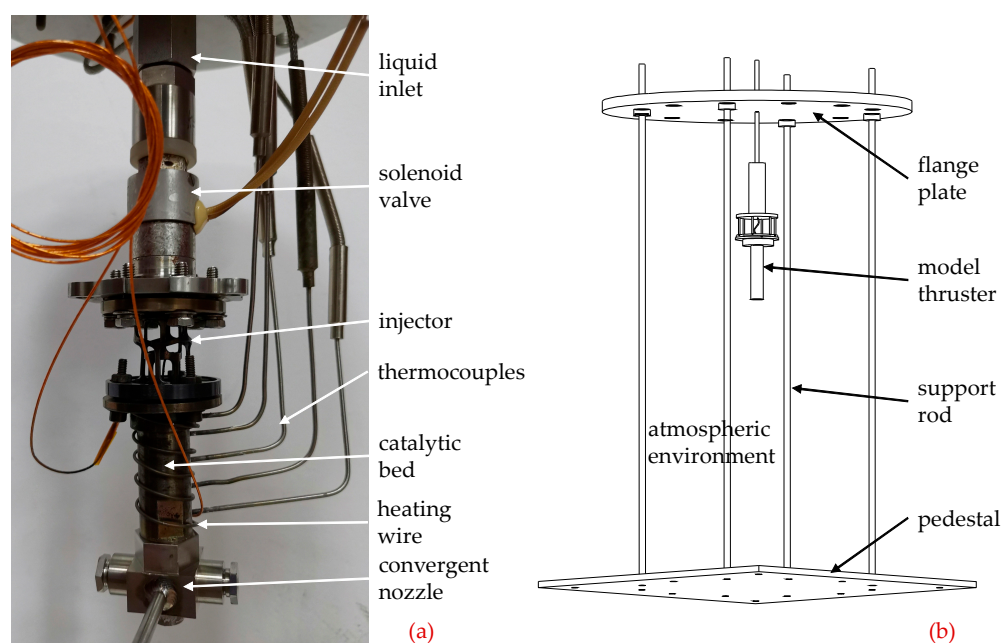


Figure 1. Model Thruster and experimental Setup: (a) model thruster; (b) experimental stand.

Figure 1b shows an atmospheric experimental stand, placed in the atmospheric environment. The main structure includes a pedestal at the bottom, four support rods, and

a flange plate on the top. The pedestal and support rods play the roles of fixing and supporting. The flange plate is placed on the support rods, and the limiters on the rods can adjust the height of the flange plate. In the center of the flange plate is welded a connecting pipe. One end below the pipe is connected with the model thruster, and the other end is connected with the propellant injection pump controlling the flow rate of the liquid propellant. Around the pipe, there are multiple terminals, through which the wirings of the thruster are uniformly connected to other equipment. At the downstream outlet of the thruster, a flue gas analyzer (Vario plus) is placed to directly measure the main gas components and their corresponding concentrations of the catalytic combustion reaction, or a gas sampling bag is placed to collect the gaseous products for later testing by gas chromatography (GC) analysis.

It should be pointed out that the flue gas analyzer has limitations on the measurement range of the corresponding components. The specific numerical range is shown in Table 1. As presented from the calibration results, the instrument had good accuracy in the measurement range. When the concentration of a gas component exceeded its measurement range, the deviation of the results increased, and the reliability of the numerical results decreased, then only the variation trend can be analyzed.

Table 1. The specific measurement range of the corresponding components.

Gaseous Product	Concentration Range	Calibration Result	
		Nominal Value \pm Tolerance Value	Actual Value
O ₂	0–20.9%	10.01 \pm 0.2%	10.05%
CO (%)	0–10%	5.02 \pm 0.15%	5.02%
CO (ppm)	0–10,000 ppm	813 \pm 40 ppm	817 ppm
CO ₂	0–20%	9.93 \pm 0.3%	9.95%
CH ₄	0–2.5%	1.973 \pm 0.06%	1.988%
NO	0–4000 pm	80.1 \pm 5 ppm	81 ppm
NO ₂	0–1000 pm	50 \pm 5 ppm	51 ppm
SO ₂	0–10,000 pm	483.4 \pm 25 ppm	486 ppm

The catalytic bed and the detachable convergent nozzle downstream of the model thruster are connected by a thread. As shown in Figure 2a, the inner diameter of the catalytic bed is 10 mm, the length is 44 mm, and there are five thermocouple sockets on one side. To measure the temperature change at different positions in the catalytic bed, five K-type thermocouples respectively recorded as TC0, TC1, TC2, TC3, and TC4 from upstream to downstream, are inserted into the centerline of the catalytic bed through the sockets. Among these thermocouples, TC0 is just at the junction where the injector connects with the catalytic bed, and the propellant will first come into contact with TC0 after entering the catalytic bed.

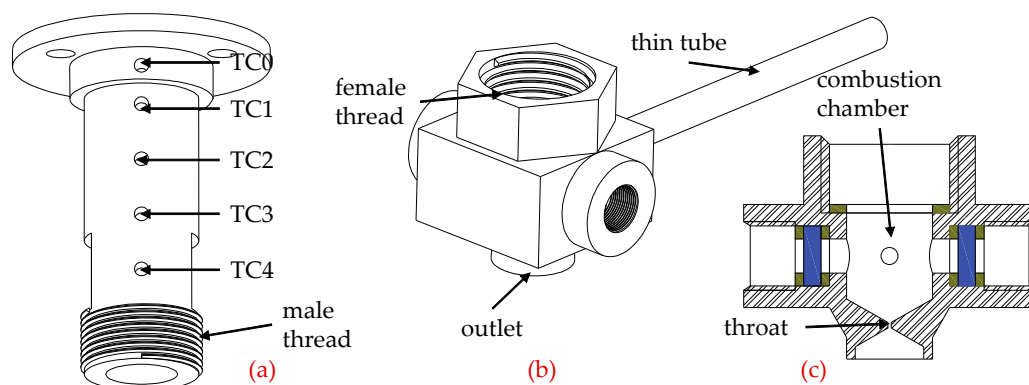


Figure 2. The catalytic and the convergent nozzle: (a) catalytic bed; (b) convergent nozzle; (c) section view of the convergent nozzle.

As shown in Figure 2b,c, inside the convergent nozzle is a combustion chamber with a diameter of 10 mm and a height of 10 mm. The diameter of the downstream throat is 0.4 mm so that the combustion chamber can be pressurized to form a high chamber pressure environment. A thin tube is welded to the outer wall of the combustion chamber, which connects to a pressure sensor (XTEH-10L-190M-14BARA-4) to acquire the pressure data inside.

The data measured by the thermocouples and the pressure sensor are recorded at 10 Hz and transmitted to the computer for display and storage. The catalytic bed will be in an atmospheric environment if the convergent nozzle is removed. Moreover, the high combustion chamber pressure environment can be realized by connecting with the convergent nozzle, as a result of which catalytic ignition experiments under different pressure environments can be accomplished by running the model thruster with or without a convergent nozzle.

Figure 3 demonstrates the preheating temperature distribution at different depths of the catalytic bed. It can be seen from the figure that the temperature in the middle stream is higher, while the temperature in the upstream and downstream is slightly lower. Except for TC4, the standard deviation of each position is about 1 °C, so the preheating operation has good repeatability.

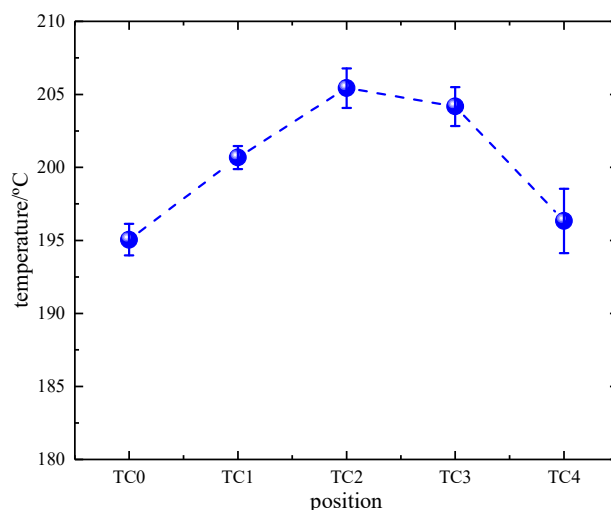


Figure 3. Preheating temperature distribution at different depths of the catalytic bed.

2.2. Experimental Procedure

The procedure of operating a model thruster without the convergent nozzle to conduct a catalytic ignition experiment in an atmospheric environment is as follows. Firstly, the catalytic bed is preheated with a heating wire, and N_2 is introduced to blow out the residual air in the catalytic bed. When the temperature of the TC0 stabilizes at 200 °C, open the solenoid valve, start the propellant injection pump to inject the dual-mode ionic liquid propellant into the model thruster at a fixed flow rate, and perform catalytic ignition in the catalytic bed. Secondly, observe the experimental phenomena and record the temperature change measured by the thermocouples at different depths. Meanwhile, a flue gas analyzer is placed at the downstream outlet to measure the gaseous products during ignition. Remove the flue gas analyzer after the combustion reaches equilibrium, turn to a gas sampling bag to collect the gas discharged from the outlet, and test with GC analysis later. Then stop the propellant feed, and blow air in so that the residual propellant in the pipeline and the incompletely reacted components in the catalytic bed can completely burn and be purged. Finishing the current operation and the next experiment can be repeated after the temperature drops. The model thruster can be preheated again and obey the same steps running the catalytic ignition experiment at the flow rate of 1~4 mL/min in sequence.

The process of using a model thruster with the convergent nozzle to carry out catalytic ignition experiments is similar to the above, but there is an additional measurement of the combustion chamber pressure in the combustion chamber. The required thrust of the propellant injection pump will increase with the build-up of the high chamber pressure, while the maximum thrust of the injection pump is limited. Therefore, only catalytic ignition experiments of 1–3 mL/min are carried out.

3. Catalytic Ignition Experiment of a Model Thruster without the Convergent Nozzle

Catalytic ignition experiments under flow rates of 1~4 mL/min were carried out in a model thruster without the convergent nozzle on the atmospheric experimental stand. Temperatures at different depths of the catalytic bed and the concentrations of several main gaseous products in the ignition progress were measured.

3.1. Variation of Catalytic Bed Temperatures

It can be seen from Figure 4a,b that under the condition of small flow rates, the temperature at TC0 rose before other downstream positions after the propellant entered the catalytic bed and contacted the preheated catalyst. Soon after the propellant reached TC0 it began to decompose to release heat. Later the TC0 temperature curve showed swift rises in two stages. The first stage rose from the initial temperature of 200 °C to around 300 °C, and then the increasing rate slowed down. The second stage rapidly rose to above 600 °C, and then gradually approached stability. Since the decomposition process of the HAN/(Emim)(EtSO₄) monopropellant exists in multiple steps [19,22], it can be inferred that the first rising stage of TC0 was due to the decomposition of the oxidant component HAN, and the second stage resulted from the decomposition of the fuel component (Emim)(EtSO₄). Moreover, the fuel component released more heat, contributing to a greater increase in the temperature curve in the second stage.

Figure 4c illustrates that at a flow rate of 3 mL/min, following the first rising stage, there was no rapid increase of the second rising stage of TC0, but it was maintained at around 300 °C. While it was TC1 that completed the second rapid ascent because the greater flow rate made the propellant flow downstream to TC1 during HAN decomposition, so (Emim)(EtSO₄) decomposed at TC1 to release a large amount of heat so that the highest temperature of TC1 exceeded 1000 °C. At about 130 s, TC1 temperature decreased slightly, and TC0 rose swiftly, did the main combustion exothermic region of the propellant beginning to move upstream.

Continuing to increase the flow rate. Figure 4d demonstrates that at a flow rate of 4 mL/min, TC0 rose rapidly in the first stage but then fell, following which TC1 ascended quickly. This was because the propellant at room temperature entered the catalytic bed with a larger flow rate and absorbed the heat at TC0 for convection. Then the fuel component accessed TC1 to decompose and released so much heat that it contributed to the second rising stage so that TC1 temperature went up swiftly to around 1200 °C. At about 260 s, TC1 to TC4 all decreased in temperature to varying degrees. However, the TC0 temperature ascended rapidly and ultimately stabilized at around 900 °C, which revealed that the main combustion exothermic region of the propellant had moved to TC0.

As mentioned above, two rising stages of the temperature curves of the catalytic bed of a model thruster without the convergent nozzle at the flow rate of 1~4 mL/min were analyzed. The characters of each stage and the maximum temperature under a separate flow rate are summarized and listed in Table 2.

3.2. Analysis of Gaseous Products of the Catalytic Ignition Process in a Model Thruster without the Convergent Nozzle

During the catalytic ignition experiment of the model thruster without the convergent nozzle in the atmospheric pressure environment, the inlet pipe of the flue gas analyzer was located at the gas outlet downstream of the catalytic bed. It identified seven gases, O₂, CO, CO₂, CH₄, SO₂, NO, and NO₂ with the analysis response frequency of 1 Hz, and

the measurement results are displayed in Figure 5. The left ordinate which shows the percentage of the gases with relatively high contents of O₂, CO, CO₂, and CH₄ is magnified ten times for better observation, while the ordinate on the right is the ppm of SO₂, NO, and NO₂ has fewer contents. Since the inlet pipe was placed in the atmospheric environment, the initial oxygen content was close to 21%, and the other gases were almost zero.

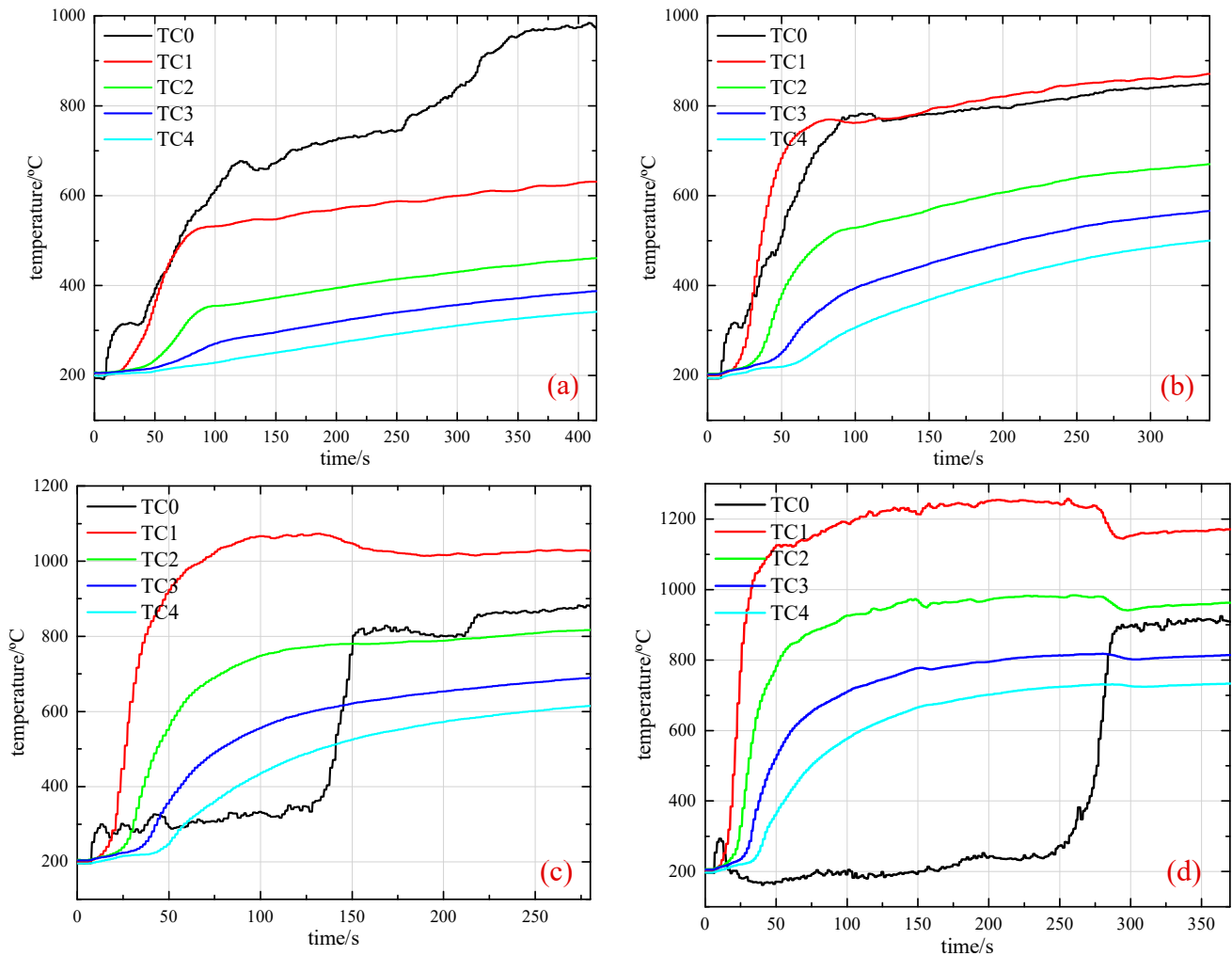


Figure 4. Temperature curves of the catalytic bed in a model thruster without the convergent nozzle at each flow rate: (a) 1 mL/min; (b) 2 mL/min; (c) 3 mL/min; (d) 4 mL/min.

Table 2. Two rising stages of the temperature curves of the catalytic bed of a model thruster without the convergent nozzle at the flow rate of 1–4 mL/min.

Flow Rate	The First Rising Stage	The Second Rising Stage	The Maximum Temperature
1 mL/min	200–310 °C, TC0 200–240 °C, TC1	320–670 °C, TC0 280–540 °C, TC1	990 °C, TC0
2 mL/min	200–320 °C, TC0 200–220 °C, TC1	300–780 °C, TC0 210–770 °C, TC1	880 °C, TC1
3 mL/min	200–300 °C, TC0 200–220 °C, TC1	around 310 °C, TC0 260–1050 °C, TC1	1070 °C, TC1
4 mL/min	200–290 °C, TC0 200–220 °C, TC1	290–160 °C, TC0 250–1100 °C, TC1	1230 °C, TC1

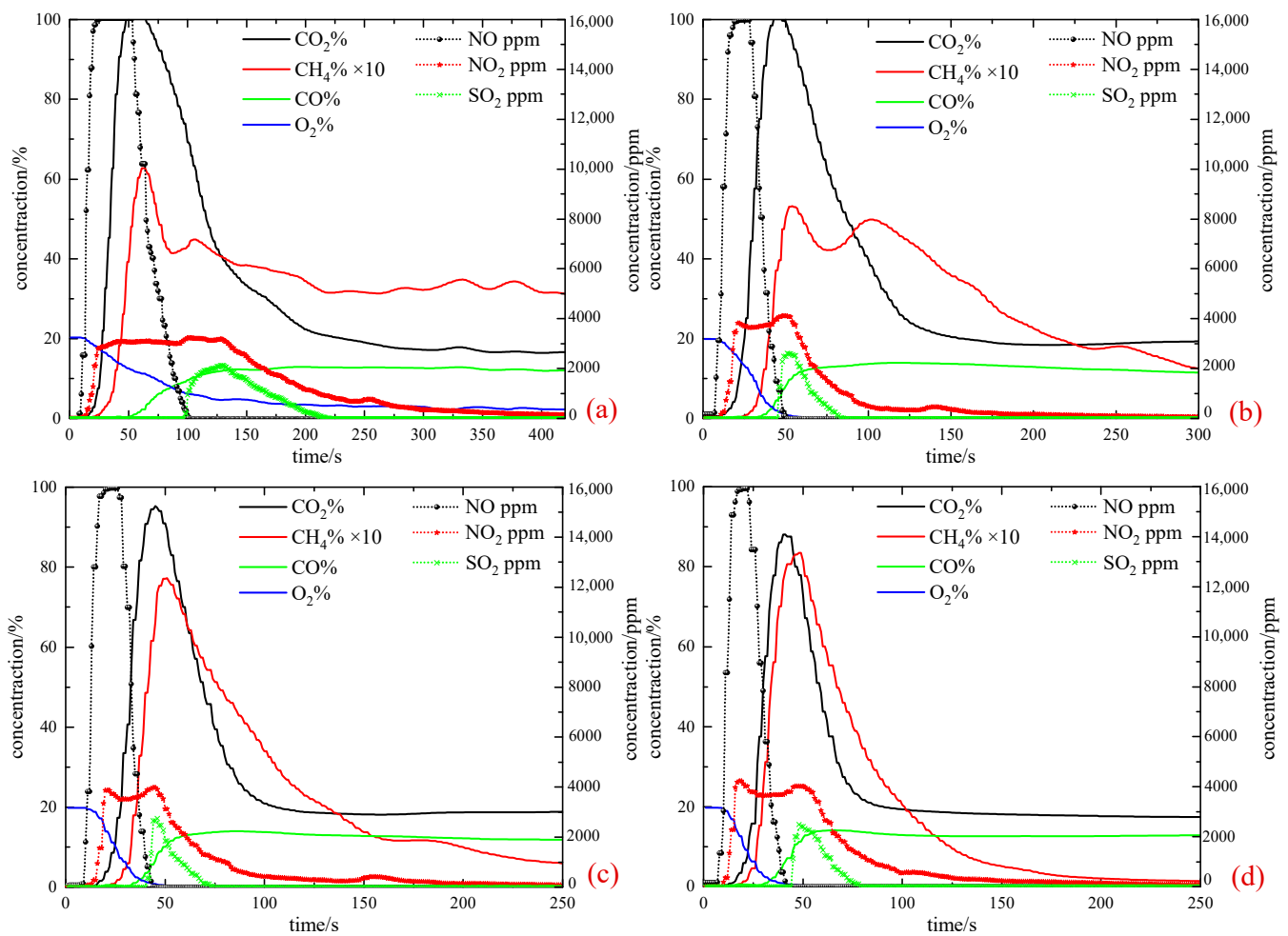


Figure 5. Flue gas analysis curves of the catalytic ignition process in a model thruster without the convergent nozzle at each flow rate: (a) 1 mL/min; (b) 2 mL/min; (c) 3 mL/min; (d) 4 mL/min.

Similar to the catalytic ignition process in a vacuum environment [24], in the initial ignition stage, the HAN of the propellant first decomposed, producing a large amount of oxidizing gas NO_x , in which the concentration of NO increased before NO_2 and its peak value went higher. Next, the C element of the $(\text{Emim})(\text{EtSO}_4)$ was oxidized into CO_2 , resulting in a significant ascent in the production of CO_2 . At the same time, NO_x was consumed, so the amount of NO quickly decreased to zero. However, after the NO_2 concentration reached a maximum value, it maintained for a while, and then faded away. With the consumption of oxidizing gas content, the incomplete combustion products of fuel components CH_4 and CO also started to appear one by one, and then the S element, with less content, was also oxidized to SO_2 . In the process of the catalytic combustion reaction tending to equilibrium, NO and SO_2 successively disappeared, but there was still a trace amount of NO_2 , while the amount of CO and CO_2 remained relatively stable. Observing the change curves of CH_4 , it can be seen that it fluctuated for a long time under a low flow rate. When approaching the reaction equilibrium, its concentration tended to be smaller as the flow rate increased.

4. Catalytic Ignition Experiment of a Model Thruster with the Convergent Nozzle

Catalytic ignition experiments under flow rates of 1–3 mL/min were conducted in a model thruster with the convergent nozzle in a high chamber pressure environment. Temperatures at different depths of the catalytic bed, the pressure of the combustion chamber, composition, and the concentrations of several main gaseous products in the ignition progress were measured.

4.1. Variation of Catalytic Bed Temperature and Combustion Chamber Pressure

Observing the enlarged part circled in Figures 6–8, it displays a small pressure peak arose at the initial stage after the propellant entered the catalytic bed. At the same time, the initial temperature of TC0 decreased slightly. Using the thermogravimetric experiments of Gao [19] and Li [22], this pattern can be judged as due to the evaporation of the water component of the monopropellant, which absorbed heat and turned into water vapor, thereby increasing the pressure.

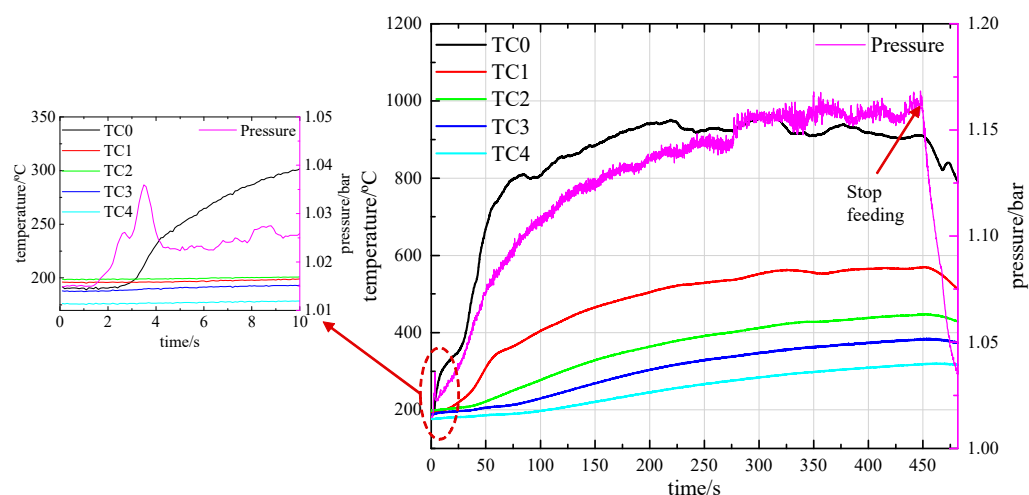


Figure 6. Temperature and pressure curves of a model thruster with the convergent nozzle at 1 mL/min flow rate.

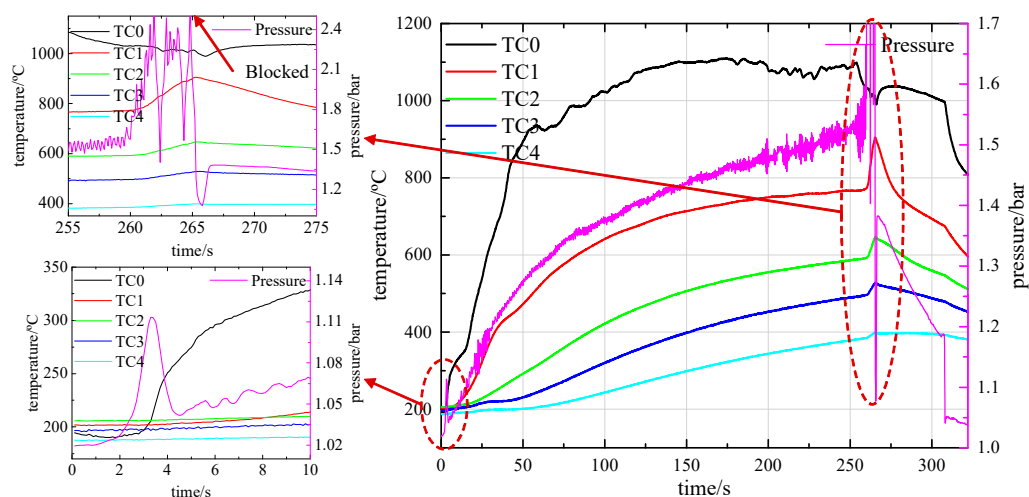


Figure 7. Temperature and pressure curve of a model thruster with the convergent nozzle at a 2 mL/min flow rate.

The temperature at TC0 rose rapidly, before the other downstream positions, while the temperature at TC1 to TC4 gradually increased. Moreover, the further away from the upstream, the slower the temperature increased. This was the result of the propellant beginning to decompose and release plenty of heat soon after contacting the catalyst, leading to a quick ascent of the temperature at TC0. Moreover, the temperature at TC0 was much higher than the temperature downstream. In other words, TC0 was the main regime where the catalytic combustion took place, while the downstream positions heated up primarily relying on the upstream heat transfer. There are also two obvious rising stages of the TC0 curve, identical to the analysis above, which respectively correspond to the decomposition of the HAN and the (Emim)(EtSO₄). The difference was that the two rising

stages arose only at TC0. The characters of each stage and the maximum temperature under the flow rate of 1~3 mL/min are listed in Table 3. The time for the end of the second rising stage was about 70 s, 55 s, and 45 s. The conclusion can be drawn that the heating rate will also accelerate with the flow rate growth.

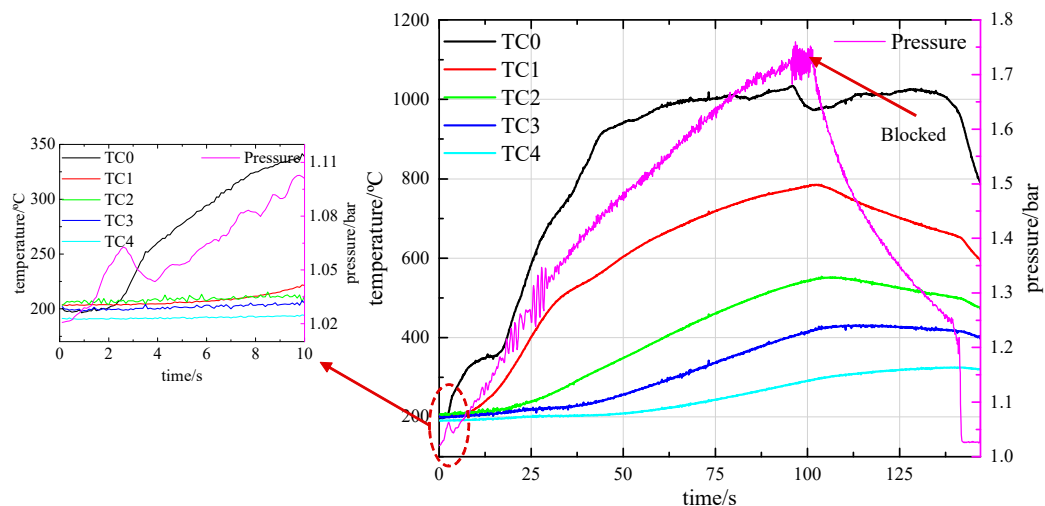


Figure 8. Temperature and pressure curve of a model thruster with the convergent nozzle at a 3 mL/min flow rate.

Table 3. Two rising stages of the temperature curves of a model thruster with the convergent nozzle at the flow rate of 1~3 mL/min.

Flow Rate	The First Rising Stage	The Second Rising Stage	The Maximum Temperature
1 mL/min	200–310 °C, TC0	350–800 °C, TC0	950 °C, TC0
2 mL/min	200–330 °C, TC0	350–930 °C, TC0	1100 °C, TC0
3 mL/min	200–350 °C, TC0	380–920 °C, TC0	1030 °C, TC0

In Figure 6, the growth rate of temperatures and pressure slowed down after about 70 s under the flow rate of 1 mL/min. The temperature of TC0 gradually rose and tended to be around 900 °C, and the pressure finally fluctuated around 1.15 bar, which was higher than the atmospheric pressure of 1.01 bar. When the propellant feeding was stopped at about 450 s, the pressure dropped linearly immediately, while the temperature drop was slightly delayed and the drop speed was relatively gentle.

In Figure 7, under the flow rate of 2 mL/min, after about 55 s, the growth rate of temperatures and pressure also slowed down, the temperature of TC0 tending to be close to 1100 °C, while the pressure continued to increase gently. At about 200 s, a gas sampling bag was added surrounding the outlet of the convergent nozzle to collect gaseous products, so that the pressure at the outlet was slowly higher than the atmospheric pressure, leading to the combustion chamber pressure fluctuating in a wider range. At 260 s, it suddenly rose from about 1.5 bar to more than 2.5 bar but then dropped to around 1.5 bar. During this period, TC1–TC4 all had a certain range of temperature rises. After a large range of fluctuation lasting about 5 s, the injection pump was blocked due to its inability to keep a certain thrust, ceasing the feed of propellant. Following that, there appeared to be two stages of cooling and depressurization. The pressure in the first stage dropped to 1.1 bar, rebounded to 1.4 bar, then decreased linearly to 1.2 bar. During this period, TC1–TC3 also set about to decrease. TC4 was far away from the upstream position of the propellant ignition, causing the slightest change. However, there emerged an increase in temperature for TC0 due to a hot reflux. This stage lasted about 40 s. At about 310 s in the second stage, the pressure plummeted to near atmospheric pressure and held steady. In this process, TC0–TC4 temperatures all accelerated their rate of decline.

Under the flow rate of 3 mL/min in Figure 8, after about 45 s, the temperature rise slowed down, and the temperature of TC0 tended to 1000 °C, but the growth rate of the pressure did not decline significantly. When the pressure reached 1.7bar, its fluctuation range enlarged. Soon after that, the propellant injection pump was blocked at about 100 s, and the propellant feeding ended. Then there existed two stages of cooling and depressurization similar to that in Figure 7. In the first stage, the pressure was reduced to around 1.2 bar. In the meantime, TC1–TC3 pressures also started to decrease, although TC4 pressure still rose inertially, while TC0 showed a certain rise due to hot reflux, which it held for about 40 s. In the second stage, from about 140 s, the pressure dropped immediately to close to atmospheric pressure and then remained constant. At the same time, TC0–TC4 pressures also accelerated their rate of decrease.

4.2. Analysis of Gaseous Products of the Catalytic Ignition Process in a Model Thruster with the Convergent Nozzle

During the catalytic ignition experiment of a model thruster with the convergent nozzle, the inlet pipe of the flue gas analyzer was located at the outlet of the convergent nozzle. The rate of the catalytic ignition can also be revealed through the change in the oxygen content. Figure 9a shows that at a flow rate of 1 mL/min, the oxygen concentration decreased gently and was always higher than zero, indicating the catalytic combustion reaction was slow at this time. The low gas production rate prevented the air around the location of the flue gas analyzer inlet pipe from being quickly purged. While in Figure 9b, it shows that at 2 mL/min and 9c 3 mL/min flow rates, the oxygen was close to disappearing at about 60 s and 50 s, respectively. These demonstrates that at the flow rate of 1~3 mL/min, with the increase of flow rate, the catalytic ignition reaction rate also be sped up.

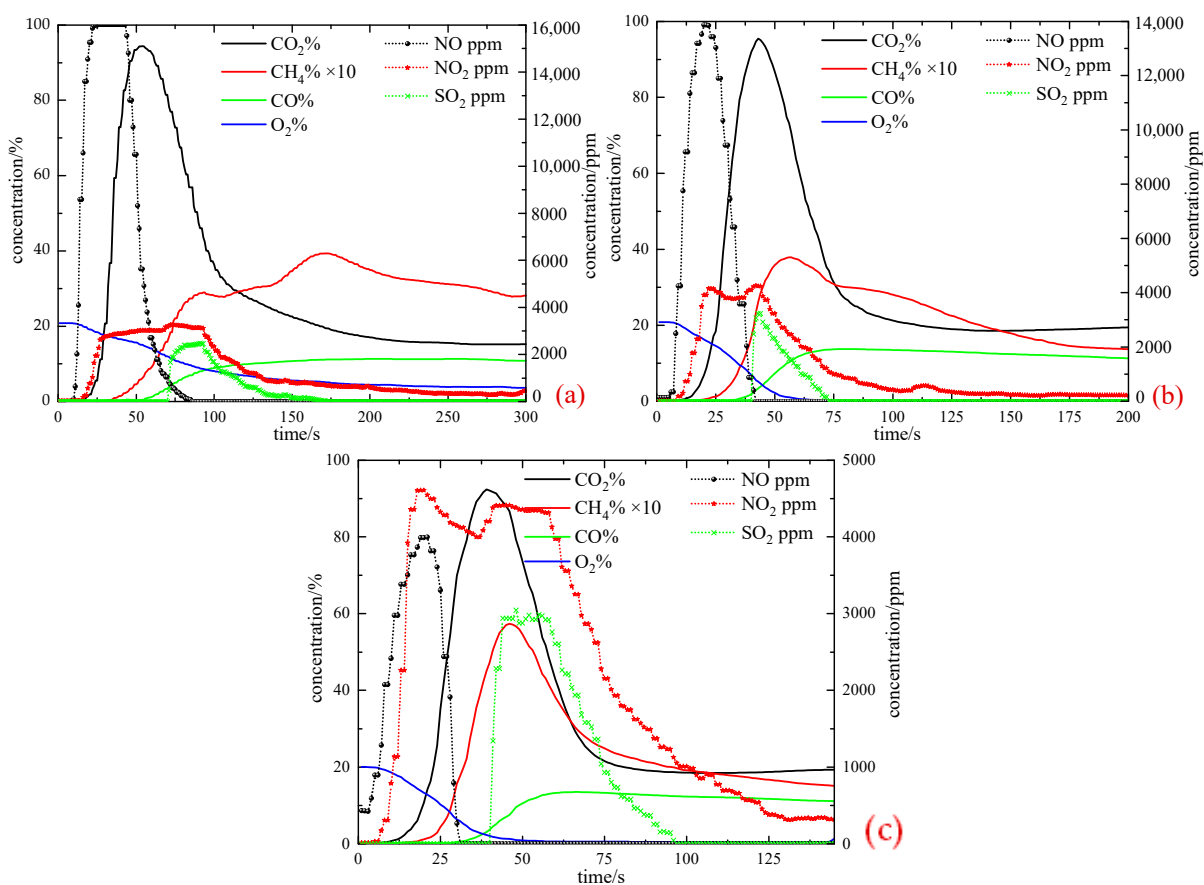


Figure 9. Flue gas analysis curves of the catalytic ignition process in a model thruster with the convergent nozzle at each flow rate: (a) 1 mL/min; (b) 2 mL/min; (c) 3 mL/min.

Similar to the catalytic ignition process of a thruster without the convergent nozzle, NO vanished in no time after peaking, while the NO₂ concentration was maintained for a time after reaching the maximum value and then gradually decreased but was not entirely consumed. Compare the maximum concentrations of NO and NO₂ in Figure 9a–c. It can be seen that increasing the flow rate reduced the NO content produced by the initial HAN decomposition, while the NO₂ content increased slightly.

5. Analysis of Gaseous Products at Equilibrium

On the one hand, the gaseous products of the catalytic combustion at equilibrium were theoretically calculated with CEA under different temperatures and different pressure. On the other hand, the exhaust gases of three groups of catalytic ignition experiments under different pressure environments were collected and measured by GC when the experiments were close to equilibrium.

5.1. Theoretical Calculation of CEA

Firstly, we used the NASA Chemical Equilibrium with Application (CEA) [27] computer code (the code for theoretical performance estimation of rocket and satellite propellants) to calculate the concentration changes of several main components of the dual-mode ionic liquid propellant at different pressures (with the temperature of 1400 K) and different temperatures (with the pressure of 1 atm), so that we could theoretically assess the contribution of pressure and temperature to reaction products. To compare with the gas chromatography (GC) analysis results of the following, CO, CO₂, CH₄, N₂, and H₂ the CEA calculation results were selected, and the concentrations of these five gases were normalized. The normalized results are presented in Figure 10.

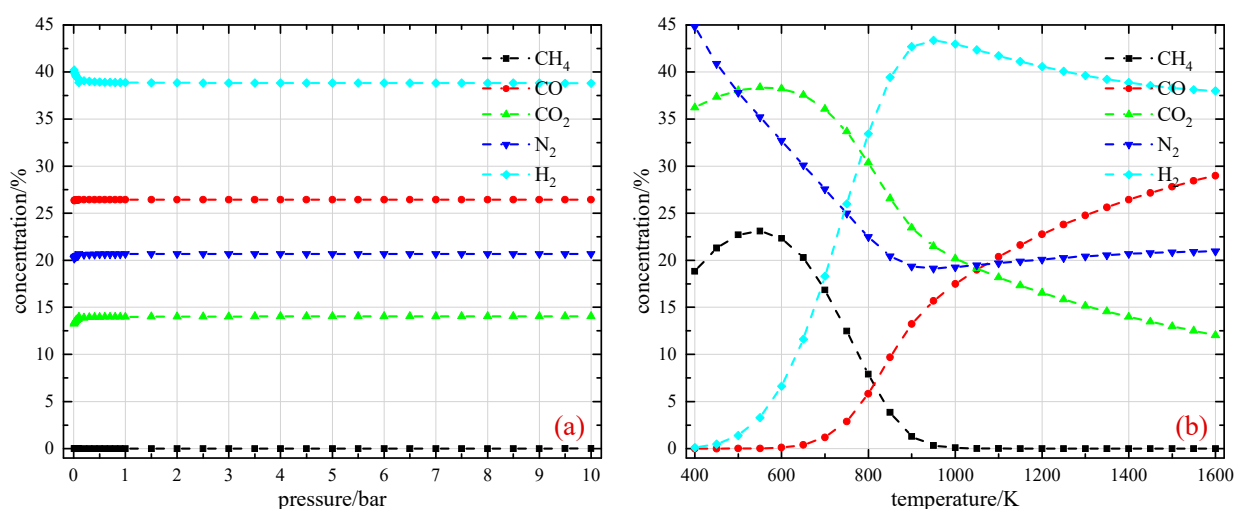


Figure 10. CEA analysis results at: (a) different pressures and; (b) different temperatures.

As can be seen in Figure 10a, at the temperature of 1400 K, the pressure had little influence on the content of these five gases at reaction equilibrium. CH₄ content was almost zero, H₂ content was the highest with a concentration close to 40%, CO content was higher than CO₂, with a sum of these two concentrations at about 40%, and the concentration of N₂ was slightly higher than 20%.

From Figure 10b, it can be seen that with a pressure of 1 atm, N₂, CH₄, and CO₂ occupied the vast majority of the contents under low temperatures, while the contents of H₂ and CO were low or even zero. Within the range of 600~900 K, the concentrations of N₂, CH₄, and CO₂ decreased, while that of H₂ and CO increased. When the temperature was greater than 900 K, CH₄ gradually disappeared. The variation tendency of N₂ and H₂ slowed down, while CO continued to increase and CO₂ continued to decrease. On the one hand, the high content of H₂ indicated an overall reducing atmosphere, so the C element

was not completely burned to produce CO. On the other hand, part of CO₂ is reduced to CO under a high-temperature environment.

The calculated values and normalized values at different temperatures are given in Table 4. The normalized value of CO, CO₂, CH₄, N₂, and H₂ was obtained by dividing the respective calculated value by the total value. Besides the selected five kinds of gases, water vapor also took up a significant proportion. The water vapor concentration was even close to half at low temperatures while the total value occupied a small amount. That's because the evaporation of water had mainly occurred, and the decomposition reaction rate of oxidant and fuel components was slow in the case of low temperature.

Table 4. The calculation value and the normalized value of CEA calculation at different temperatures.

T (K)	Calculation Value (%)						Normalized Value (%)					
	CH ₄	CO	CO ₂	H ₂	N ₂	Total ¹	H ₂ O	CH ₄	CO	CO ₂	H ₂	N ₂
400	6.566	0	12.63	0.044	15.625	34.865	49.818	18.833	0	36.225	0.126	44.816
500	9.949	0.002	16.658	0.607	16.558	43.774	46.254	22.728	0.005	38.055	1.387	37.826
600	11.605	0.058	19.881	3.445	17.014	52.003	41.948	22.316	0.112	38.23	6.625	32.717
700	10.157	0.716	21.737	11.039	16.613	60.262	35.646	16.855	1.188	36.071	18.318	27.568
800	5.376	3.959	20.664	22.757	15.293	68.049	28.185	7.9	5.818	30.366	33.442	22.474
900	0.937	9.611	17.025	30.999	14.068	72.64	23.899	1.29	13.231	23.438	42.675	19.367
1000	0.058	12.534	14.492	30.832	13.827	71.743	24.861	0.081	17.471	20.2	42.976	19.273
1100	0.004	14.284	12.756	29.251	13.813	70.108	26.501	0.006	20.374	18.195	41.723	19.702
1200	0.001	15.654	11.379	27.898	13.812	68.744	27.869	0.001	22.771	16.553	40.582	20.092
1300	0	16.756	10.267	26.812	13.81	67.645	28.976	0	24.77	15.178	39.636	20.415
1400	0	17.655	9.354	25.962	13.806	66.777	29.872	0	26.439	14.008	38.879	20.675
1500	0	18.402	8.585	25.339	13.795	66.121	30.594	0	27.831	12.984	38.322	20.863
1600	0	19.038	7.913	24.947	13.774	65.672	31.16	0	28.990	12.049	37.987	20.974

¹ This is the sum of the theoretical value of CH₄, CO, CO₂, H₂, and N₂.

5.2. GC Analysis of the Exhaust Gas

Based on the CEA theoretical calculation, the exhaust gases of the catalytic ignition under the vacuum environment, the atmosphere, and a high chamber pressure environment were separately collected with gas sampling bags when the maximum temperature measured stabilized. The GC analysis of these gases is presented in Figure 11. The maximum temperature was chosen because it was where the reaction mainly occurred. Among the three groups of experiments, the catalytic ignition experiment in the vacuum environment has been reported in the literature [24], and the temperature curves are displayed in Figure 11.

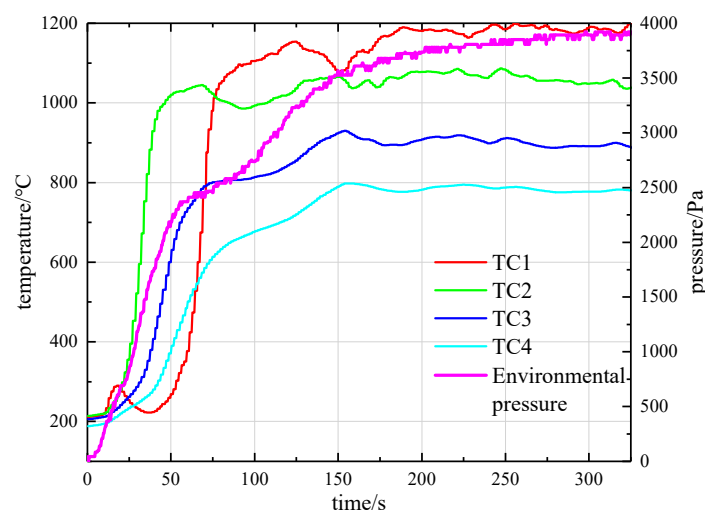


Figure 11. Temperature and pressure curves of a model thruster without the convergent nozzle carrying on the catalytic ignition experiment in the vacuum environment.

The experiment in the atmosphere was conducted in the model thruster without the convergent nozzle, and the experiment in the high chamber pressure environment was conducted in the model thruster with the convergent nozzle as described in Figures 4c and 8 above. All of them were carried out at a preheating temperature of 200 °C and a feeding flow rate of 3 mL/min. It should be noticed that even though the catalytic ignition experiments approached equilibrium, the pressure and the temperature still fluctuated to a certain extent. Moreover, there existed differences in the temperature at different depths of the catalytic bed. Since the water vapor condensed into liquid water in gas sampling bags, we measured the main components including CO, CO₂, CH₄, N₂, and H₂, without water vapor, and the results were normalized.

As was shown in Figure 12, N₂ and H₂ occupies about 70%, and the three pressure environments had little effect on their concentration, which conformed to the analysis from Figure 10a, but the concentration of carbonaceous matter appeared with some differences. The content ratio of CO₂ and CO, i.e., $c(\text{CO}_2/\text{CO})$, was the lowest at 0.92 in the vacuum environment and the highest at 1.56 in the high chamber pressure environment. In addition, the GC results showed that no CH₄ was detected in the vacuum environment, while a small amount of CH₄ was produced in the atmosphere and took up a larger proportion in the high chamber pressure environment.

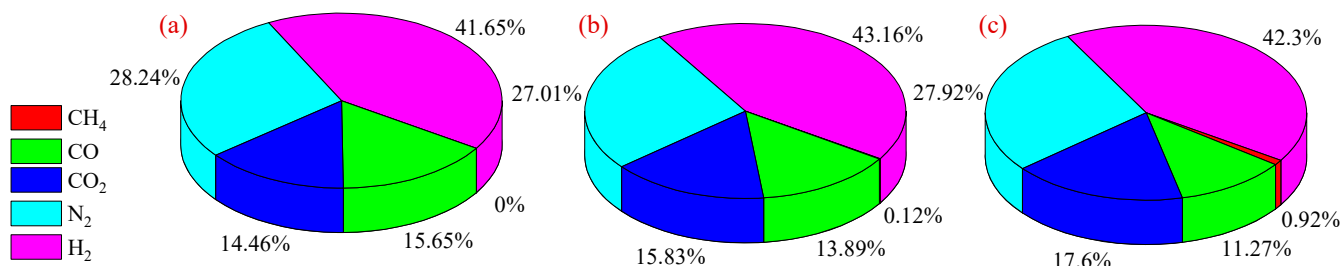


Figure 12. The results of GC analysis in different pressure environments: (a) vacuum environment; (b) atmospheric environment; (c) high chamber pressure environment.

5.3. Comparison of Theoretical Calculation and Experimental Results

Figure 13 demonstrates a comparison of the theoretical calculation and the experimental results. Because the whole temperature of the catalytic bed when approaching equilibrium in a vacuum environment in Figure 11 was the highest, while that in a high chamber pressure environment in Figure 8 was the lowest and its ignition time was the shortest leading to the other temperatures downstream being still on the rise even though the maximum temperature was close to stability. Combining these above features of the analytical and measured results, it can be judged that the three groups of experimental results roughly coincide with the position of 1100 K, 1000 K, and 900 K respectively of the CEA calculation in Figure 10b. As shown in Figure 13, the concentrations of H₂ and CH₄ measured with GC agreed well with that of the theoretical calculation. Though the experimental value of N₂ was higher than the theoretical value, and the experimental values of CO and CO₂ were lower, their trends were consistent with that of the theoretical calculation.

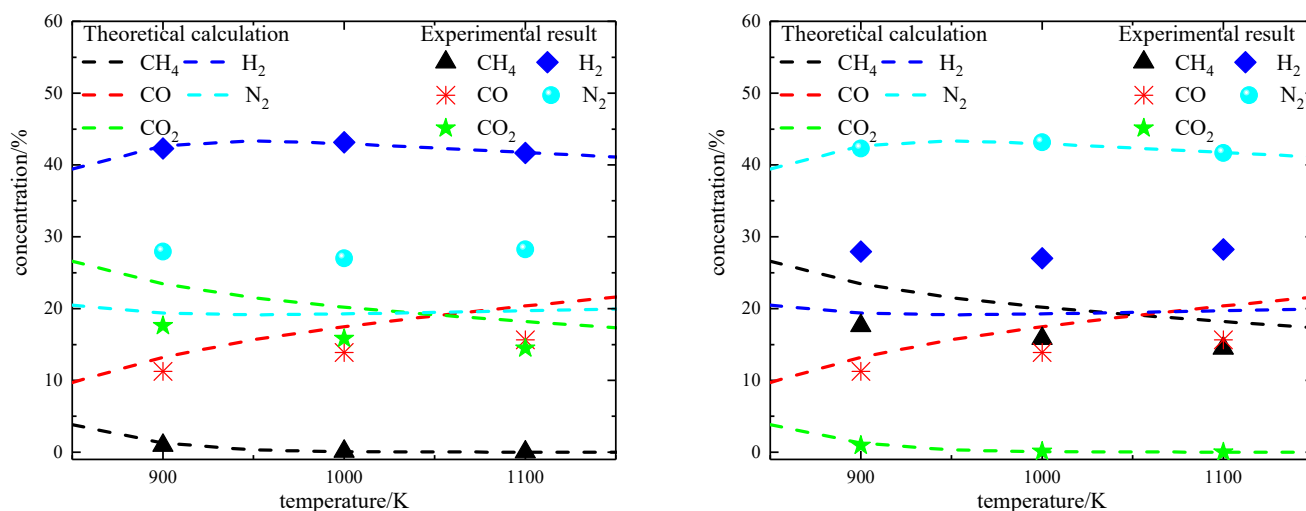


Figure 13. Comparison of theoretical calculation and experimental results.

6. Conclusions

In this paper, catalytic ignition experiments of the HAN/(Emim)(EtSO₄) dual-mode ionic liquid monopropellant were carried out under the flow rates of 1~4 mL/min and 1~3 mL/min respectively using a model thruster without and with the convergent nozzle at a preheating temperature of 200 °C. From the measurements of temperature at different depths of the catalytic bed, the pressure of the combustion chamber, and the main components of the gaseous products and their corresponding concentrations, as well as theoretical calculation of CEA and GC analysis of exhaust gas, the following conclusions can be drawn:

- (1) When the propellant flows into the catalytic bed, the H₂O component evaporates first, causing a small pressure peak in the combustion chamber pressure, which can be observed in a model thruster with the convergent nozzle.
- (2) Secondly the temperature curves appear in two rising stages respectively corresponding to the decomposition of the oxidant component HAN and the fuel component (Emim)(EtSO₄) in both a model thruster without and with the convergent nozzle. In a model thruster with the convergent nozzle, the two rising stages are directly completed at the position where the propellant first contacts it after the propellant is injected into the catalytic bed. The HAN decomposes at the same depth in a model thruster without the convergent nozzle while the position (Emim)(EtSO₄) decomposes will move downstream as the flow rate increases.
- (3) In addition, the decomposition of the HAN will produce the oxidizing gas NO_x. Then (Emim)(EtSO₄) starts to fully react with NO_x, depleting NO immediately. In the meantime, the C element is oxidized to CO₂ in a large amount, letting out plenty of heat. In this process CH₄, CO, and SO₂ are also produced. Following that, the temperature tends to be stable, NO_x is completely reacted, SO₂ is no longer generated, CH₄ will slowly decrease and even disappear, and the concentrations of CO and CO₂ gradually reach stability in the process of approaching the equilibrium.
- (4) When the catalytic ignition approaches equilibrium, the analytical results of GC are consistent with the trend of theoretical calculation by CEA. The ambient pressure has little influence on exhaust gas; however, the temperature is a significant factor. The contents of N₂ and H₂ occupy the majority, and that of CH₄, CO₂, and CO are determined by the temperature.

Author Contributions: Conceptualization, J.F., H.G., Z.Y. and S.L.; methodology, J.F. and Z.W.; formal analysis, J.F. and Z.Y.; investigation, J.F., Z.W., H.Y., H.G., Z.Y. and S.L.; resources, J.F. and Z.Y.; data curation, J.F.; visualization, J.F.; writing—original draft preparation, J.F.; writing—review and editing, J.F., H.Y., Z.Y. and S.L.; supervision, Z.Y. and S.L. All authors have read and agreed to the published version of the manuscript.

Funding: This research received no external funding.

Data Availability Statement: Not applicable.

Conflicts of Interest: The authors declare no conflict of interest.

References

1. Rovey, J.L.; Lyne, C.T.; Mundahl, A.J.; Rasmont, N.; Glascock, M.S.; Wainwright, M.J.; Berg, S.P. Review of chemical-electric multimode space propulsion. In Proceedings of the AIAA Propulsion and Energy 2019 Forum, Indianapolis, IN, USA, 19–22 August 2019.
2. Coleman, D.; Benedict, M.; Hrishikeshavan, V.; Chopra, I. Design, development, and flight-testing of a robotic hummingbird. In Proceedings of the American Helicopter Society 71st Annual Forum, Virginia Beach, VA, USA, 5–7 May 2015.
3. Lazurenko, A.; Vial, V.; Bouchoule, A.; Skrylnikov, A.; Kozlov, V.; Kim, V. Dual-mode operation of stationary plasma thrusters. *J. Propuls. Power* **2006**, *22*, 38–475. [[CrossRef](#)]
4. Rovey, J.L.; Lyne, C.T.; Mundahl, A.J.; Rasmont, N.; Glascock, M.S.; Wainwright, M.J.; Berg, S.P. Review of multimode space propulsion. *Prog. Aerosp. Sci.* **2020**, *118*, 100627. [[CrossRef](#)]
5. Donius, B.R.; Rovey, J.L. Ionic liquid dual-mode spacecraft propulsion assessment. *J. Spacecr. Rocket.* **2011**, *48*, 110–123. [[CrossRef](#)]
6. Zhang, Q.; Shreeve, J.N.M. Energetic ionic liquids as explosives and propellant fuels: A new journey of ionic liquid chemistry. *Chem. Rev.* **2014**, *114*, 10527–10574. [[CrossRef](#)] [[PubMed](#)]
7. Donius, B.R.; Rovey, J.L. Analysis and prediction of dual-mode chemical and electric ionic liquid propulsion performance. In Proceedings of the 48th AIAA Aerospace Sciences Meeting Including the New Horizons Forum and Aerospace Exposition, Orlando, FL, USA, 4–7 January 2010.
8. Romero-Sanz, I.; Bocanegra, R.; Fernandez De La Mora, J.; Gamero-Castano, M. Source of heavy molecular ions based on Taylor cones of ionic liquids operating in the pure ion evaporation regime. *J. Appl. Phys.* **2003**, *94*, 3599–3605. [[CrossRef](#)]
9. Garoz, D.; Bueno, C.; Larriba, C.; Castro, S. Taylor cones of ionic liquids from capillary tubes as sources of pure ions: The role of surface tension and electrical conductivity. *J. Appl. Phys.* **2007**, *102*, 064913. [[CrossRef](#)]
10. Sutton, G.P.; Biblarz, O. *Rocket Propulsion Elements*; John Wiley & Sons: New York, NY, USA, 2016.
11. Berg, S.P.; Rovey, J.L. Dual-mode propellant properties and performance analysis of energetic ionic liquids. In Proceedings of the 50th AIAA Aerospace Sciences Meeting including the New Horizons Forum and Aerospace Exposition, Nashville, TN, USA, 9–12 January 2012.
12. Berg, S.P.; Rovey, J.L. Ignition evaluation of monopropellant blends of HAN and imidazole-based ionic liquid fuels. In Proceedings of the 50th AIAA Aerospace Sciences Meeting including the New Horizons Forum and Aerospace Exposition, Nashville, TN, USA, 9–12 January 2012.
13. Berg, S.P.; Rovey, J.L.; Prince, B.; Miller, S.; Bemish, R. Electro spray of an energetic ionic liquid monopropellant for multi-mode micropropulsion applications. In Proceedings of the 51st AIAA/SAE/ASEE Joint Propulsion Conference, Orlando, FL, USA, 27–29 July 2015.
14. Berg, S.P.; Rovey, J.L. Decomposition of a double salt ionic liquid monopropellant on heated metallic surfaces. In Proceedings of the 52nd AIAA/SAE/ASEE Joint Propulsion Conference, Salt Lake City, UT, USA, 25–27 July 2016.
15. Mundahl, A.J.; Rovey, J.L.; Berg, S.P. Linear burn rate of monopropellant for multi-mode micropropulsion. In Proceedings of the 2018 Joint Propulsion Conference, Cincinnati, OH, USA, 9–11 July 2018.
16. Berg, S.P.; Rovey, J.L. Decomposition of a Double Salt Ionic Liquid Monopropellant in a Microtube for Multi-Mode Micropropulsion Applications. In Proceedings of the 53rd AIAA/SAE/ASEE Joint Propulsion Conference, Atlanta, GA, USA, 10–12 July 2017.
17. Berg, S.P.; Glascock, M.S.; Cooper, M.; Rovey, J.L. Multimode Integrated Monopropellant Electro spray Thruster Testing Results: Chemical Mode. In Proceedings of the NASA In-Space Chemical Propulsion Technical Interchange Meeting, Online, 14–17 September 2020.
18. Lyne, C.T.; Rovey, J.; Berg, S.P. Monopropellant-Electro spray Multimode Thruster Testing Results: Electro spray Mode. In Proceedings of the AIAA Propulsion and Energy 2021 Forum, Virtual Event, 9–11 August 2021.
19. Wang, W.; Ma, Z.; Cong, W.; Zhang, W.; Xia, L.; Wang, X. Studies on Synthesis, Characterization and Catalytic Decomposition of Multitask Mode Ionic Liquid Propellant. *J. Propuls. Technol.* **2020**, *41*, 455–460. (In Chinese)
20. Gao, H.; Li, S.; Yao, Z.; Li, S. Experimental Study on Thermal and Catalytic Decomposition of a Dual-Mode Ionic Liquid Propellant. *E3S Web Conf.* **2021**, *257*, 01041. [[CrossRef](#)]
21. Sharma, A.; Adducci, A.C.; Rovey, J.; Ma, C.; Ryan, C.N.; Berg, S. Green Ionic Liquid Multimode Monopropellant Based Chemical Micro-thruster. In Proceedings of the AIAA SCITECH 2022 Forum, San Diego, CA, USA, 3–7 January 2022.

22. Li, S.; Yan, H.; Wang, Z.; Tang, Y.; Yao, Z.; Li, S. Catalytic Decomposition and Burning of a Dual-Mode Ionic Liquid Propellant. *Energy Fuels* **2021**, *35*, 18716–18725. [[CrossRef](#)]
23. Tang, Y.; Li, S.; Yao, Z.; Huang, B.; Li, S. Ignition of an ionic dual-mode monopropellant using a microwave plasma torch. *Proc. Combust. Inst.* **2022**, in press. [[CrossRef](#)]
24. Fang, J.; Wang, Z.; Yan, H.; Gao, H.; Yao, Z.; Li, S. Catalytic Ignition Characteristics of Dual-mode Ionic Liquid Propellant under Vacuum Condition. *J. Rocket. Propuls.* **2022**, *48*, 1–8. (In Chinese)
25. Schneider, S.; Hawkins, T.; Rosander, M.; Vaghjiani, G.; Chambreau, S.; Drake, G. Ionic liquids as hypergolic fuels. *Energy Fuels* **2008**, *22*, 2871–2872. [[CrossRef](#)]
26. Weng, X.; Tang, C.; Li, J.; Zhang, Q.; Huang, Z. Coulomb explosion and ultra-fast hypergolic ignition of borohydride-rich ionic liquids with WFNA. *Combust. Flame* **2018**, *194*, 464–471. [[CrossRef](#)]
27. McBride, B.J.; Gordon, S. *Computer Program for the Calculation of Complex Chemical Equilibrium Compositions and Applications II. User's Manual and Program Description*; National Aeronautics and Space Administration (NASA): Washington, DC, USA, 1996. Available online: <https://ntrs.nasa.gov/citations/19960044559> (accessed on 16 June 2021).